(2)

DEVELOPMENT OF THE MICROSTRUCTURE BASED STOCHASTIC LIFE PREDICTION MODELS

Quarterly Report
ONR Grant No: N00014-91-J-1299

Submitted to:

Dr. *A. K. Vasudévan*
Technology Directorate
Code 4421
Office of Naval Research
800 North Quincy Street
Arlington, VA 22217-5660

Prepared by :

Professor *Marek A. Przystupa* (Principal Investigator)
Jimin Zhang
Annetta J. Luévano
Department of Material Science and Engineering
University of California
Los Angeles, CA 90024
Tel.: (310) 825-6559
FAX: (310) 206-7353

September, 1993

Table of Contents

ABSTRACT

The microstructural features of 7050 T7451 aluminum alloy in the vicinity of fatigue cracks and on the crack path were studied to determine which of them influence fatigue crack propagation. The studies included characterization of the full spectrum of microstructural and fracture surface features starting from the largest ones such as roughness and grain type to the smallest such as second phase particles and dislocations. Of all the features studied, only the second phase particles were shown to have a definite influence by causing crack deflection. The number of particles encountered by the fatigue cracks were significantly higher than the expected average. The fatigue crack path was predominately transgranular and there was no changes in the dislocation and precipitation structures in the crack affected zone.

1. Introduction

Fatigue failures in metals and alloys are always preceded by the accumulation of microstructural damage. Such damage manifests itself as microcracking, debonding, development of slip bands, formation of dislocation cell structures and, ultimately, as the nucleation and growth of a fatigue crack. The sequences of damage accumulation events leading to the fatigue crack nucleation and growth are still debatable, but there is no doubt that the fatigue resistance is low in alloys susceptible to large amounts of microstructural damage[1]. In order to improve fatigue resistance and/or to formulate realistic life prediction models it is thus necessary to determine which forms of damage take place in different alloys and to rank their importance.

The purpose of this work was to identify microstructural damage processes taking place during fatigue in a typical precipitation hardened aluminum aerospace plate alloys and to assess their importance in controlling crack propagation rates. The aluminum alloys have been chosen because of their prominence in aerospace applications. These alloys also have very complex structures consisting of unrecrystallized or partially recrystallized grains with matrix and grain boundary precipitates, constituent particles, microporosities and, in many instances, precipitation free zones[2,3,4,5]. The dominant fatigue cracks usually starts from the largest surface micropore and propagates tortuously through the matrix . The crack deflections results from the linking-up of the main crack with the microcracks in the damage zone preceding it or to the preferred intergranular fracture, cracking along slip planes, etc. Each of those causes constitutes different type of microstructural damage mechanisms and the one that is actually active can be identified from metallographic and fractographic examinations. The results of such an analysis, for the 7050-T7451 plate alloy, are reported in this report. They include information about the crack geometry, distribution of different futures on the crack path and on the microstructural damage inflicted during fatigue.

2. Experimental Procedure

The material used in this study was from the center of a batch of 7050-T7451 14.5 cm thick plate alloy designated as "old quality" by Alcoa. This alloy, Figure 1, is 20 % recrystallized and contains, by volume, about 0.1 % of porosities and 0.65 % of constituent particles in the form of stringers[6]. Their average sizes are 3.4 and 4.5 μm respectively [6]. The precipitate microstructure consists of grain boundary and matrix precipitates which are shown in Figures 2a and b respectively. The matrix precipitates have been identified as η' and η, while the grain boundary precipitates are predominately η. Since the alloy has been partially recrystallized, the dislocations are not apparent in these microstructures.

The samples for damage assessment used in this investigation were cut from two-hole fatigue specimens shown in Figure 3a. Two-hole specimens were used to simulate the loading condition similar to those of bolt holes in an aircraft part [3,4,5]. They were cut from the center section of a plate with the long axis normal to the rolling direction. The two-hole specimens were then fatigued to failure under the conditions of σ_{max} = 170 MPa, R = 0.1 and frequency of 10 Hz. In all cases the cracking started from large surface micropores[5]. Some of the failed samples contained secondary fatigue cracks at the unfailed hole (Fig. 3b). These cracks are ideal for identifying the microstructural features on both sides of the fatigue crack path. The microstructures in the vicinity of two such cracks that formed on opposite sides of the same hole were studied in this investigation. Both scanning (SEM) and transmission electron microscopes (TEM) were used in the examinations.

The SEM examinations were used to determine 1) the crack roughness, 2) the relationship of the crack path to grain structure, 3) the number of second phase particles

intercepts and 4) the severity of microcracking. The microstructures were characterized along two crack paths, Fig 3b, at the surface sections and at the fatigue sample 1/3 and 2/3 thickness. Scanning electron microscopy photographs in both etched and unetched conditions were used for all the measurements. Actual crack lengths and the fractions of the cracks' path through various regions (i.e. unrecrystallized grains, recrystallized grains, and grain boundaries) were measured on the micrographs using a digitizer.

One of the cracks was analyzed using a computerized system for fractographic analysis. This system allows for automatic estimation of the actual and projected crack lengths, roughness parameters, the distribution of the angles describing orientations of crack segments and the fractal dimension. The general concept of the fractal analysis has been based on the principle that the number of ruler lengths, N, required to measure the length of a curve depends on the size of the ruler, ρ, used in the measurement. A small ruler resolves finer details than a large one, but at the same time requires a disproportionately greater number of steps to cover the analyzed curve. A plot of log(N) vs. $\log(1/\rho)$ for a fractal curve yields a straight line which can be described by the relation

$$N = k\left(\frac{1}{\rho}\right)^{d}$$

where d is called the fractal dimension and k is a constant. Such defined fractal dimension gives an indication of the roughness of a surface: the closer the number is to 1, the smoother the surface. This method of defining fractal has been proposed by Mandelbrot [7].

To determine if fatigue crack deflects toward constituent particles the average numbers of particles per unit length of a straight line have been compared with the actual number of particles per unit crack length. In both measurements the enlarged photographs of the entire crack length were used. The measurements of the expected number of particles for a straight crack have been made using a scan grid of parallel lines spaced 0.5

cm apart. Because of the anisotropy of constituent particle spatial distribution the grid was always aligned with the average direction of crack propagation. Alternatively, the number of constituent particle intercepts per unit length along the actual crack path have been calculated from the measurements of the actual crack lengths and total number of particles intersected by the crack.

The SEM studies were supplemented by the TEM examination to determine if there was any change in dislocation structure in the vicinity of the crack path. Specifically, the evidence of dislocation activities in or near the cyclic plastic zone was studied. The samples for this purpose were cut from various sections along the fatigue crack path. Each TEM sample contained either starting, middle or end regions of the fatigue crack. The samples were dimpled using a solution of 10 % nitric acid and 90 % water at room temperature and a voltage of 25 V. Final polish and perforation was done with a solution of 30 % nitric acid and 70 % methanol at a temperature of -30 °C and a voltage of 15 - 18 V.

3. Results and Discussion

3.1 Roughness and Crack Geometry

The results of the crack length measurements and the profile roughness parameters, defined as the ratios of the actual to the projected crack lengths, have been summarized in Table 1. As expected, the projected crack lengths in the interior of the samples are longer than those at the surface due to the curved crack front profile. The roughness parameters varied between 1.1 and 1.24, which is in agreement with the average roughness parameter of 1.2 obtained in the parallel studies for the actual fatigue fracture surfaces of the investigated sample using fractal analysis [6].

Profi'es of the crack #2 at the surface section opposite that used in the table have been analyzed using automated fractographic and fractal analysis system. Both the upper and the lower surfaces of the crack have been analyzed. The crack length for the upper profile was 3128 μm and for the lower one it was 3028 μm. Roughness parameters were 1.2707 and 1.2535 respectively. The difference in the roughness parameters was thus only 1.35%. The results of the fractal analysis for that crack are shown in Figure 4 where the slopes of the curves represent fractal dimensions. The obtained fractal dimensions were 1.0411 and 1.0372 for the upper and lower profiles. The difference in this case is only 0.4 % which can be considered as insignificant. The results indicate that it is only necessary to study one of the profiles.

The distributions of the crack segment orientations for the upper profile of the crack #2 is shown in Figure 5. As expected, the most frequent angle for the upper profile is at about 90°, which is the general crack propagation direction. The lower profile shows a similar symmetrical trend. The distributions is relatively flat, which means that there is considerable amount of crack deflection in both profiles.

In addition to the main fatigue cracks two other types of cracks have been also observed in the studied specimens. The most frequent one of them was crack branching, shown in Figure 6. In many instances the branches grew towards and into constituent particles and/or extended along both grain and subgrain boundaries adjacent to the crack. There were also microcracks observed near, but separate from the main crack. Two examples of such microcracks are shown in Figure 7. Both of them have been located near the end of the fatigue crack and the one shown in Fig. 7a originated at a constituent particle. This means that the growth of fatigue crack in the 7050-T7451 alloy is preceded by the microcracking ahead of the crack tip with the constituent particles serving as the potential microcrack nucleation sites. The crack then propagates towards the microcracks resulting in noticeable amount of crack deflection.

3.2 Grain Structure

The interaction of the fatigue crack with grains was evaluated based on the measurements of the fractions of the length of the crack that passed through the various types of grains and/or grain boundaries. Since the material was partially recrystallized, the possible grains encountered by the crack were either recrystallized or unrecrystallized with subgrains. The lengths of the crack path along boundaries and through each type of grains were measured from the micrographs and used in the calculation of the percentages. Intergranular portions of the crack path were separated into following categories depending on the types of grain on either side of the crack: (1) unrecrystallized/ recrystallized, (2) recrystallized/recrystallized and (3) unrecrystallized/unrecrystallized. The results, Table 2, indicate that the crack propagates both transgranularly and intergranularly with the preference toward a transgranular fracture mode. The transgranular part of the crack is primarily through the unrecrystallized grains which is not unexpected as the material is only 20 % recrystallized. The fractions of the recrystallized grains encountered by the crack vary widely, but they are on the average lower than the recrystallization levels.

Intergranular failures constituted between 6 to 40 % of the total fatigue crack path. From the possible combinations, the boundaries between unrecrystallized and recrystallized grains were most frequently chosen by the crack. This implies that they are the most susceptible to the fatigue damage. It was also observed that some of the transgranular cracks in the unrecrystallized grain propagated along subgrain boundaries. The percentages of crack path along subgrain boundaries in the unrecrystallized grains are also listed Table 2. The numbers indicate that only a small percentage of the crack path followed subgrain boundaries. In the case of crack #2, the crack was open too wide to accurately determine its path.

3.3 Second Phase Particles

To determine the influence of the constituent particles on the crack path deflections the expected number of particle intercepts for the straight line have been compared with the number of particles intercepted by the actual crack path. As described earlier, the measurements were taken from the enlarged photographs, such as the one in Figure 8, to enhance the details. The results are summarized in Table 3. For each section the number of particle intercepted by the crack is always greater than the expected average for the straight line. To determine if the values are significantly different, a test of the null hypothesis that they are the same, using Student t-distribution, has been used [8]. In all cases the null hypothesis had to be rejected at the significance level less than 0.1%. This means that there is less then 0.1% chance that the number of particles intercepted by the crack is the same as that for the straight line (the actual calculated probability is even smaller and is in the 1×10^{-10} % range).

It is thus justifiable to conclude that the constituent particles do affect the crack path by causing crack deflections. The most likely reason for this behavior is particle cracking. As shown in Fig. 7, some of the particles in the vicinity of the fatigue crack path had microcracks. Such particles always attract the main fatigue crack causing crack deflections. Since the investigated 7050 has broken constituents to start with [9,10] it is not possible to tell which of the particles fractured as a result of fatigue. However, the number of particles intersected by the fatigue crack is significantly larger that the number of broken particles observed in the starting material. This means that fatigue of the 7050 alloy results in constituent particle cracking in the crack affected zone.

3.4 Precipitates and Dislocations.

Both precipitate and dislocation microstructures in the vicinity of the crack were examined and compared to that of the bulk material to establish if there was any damage due to fatigue. Since the studied material was subjected to high cycle fatigue, the most probable region, if any, where the damage would occur was in the reversible plastic zone. To determine the size of that zone and thus to find out how close to the fatigue crack the TEM sample had to be perforated, the following equation has been used [1]:

$$r_c = \frac{1}{\pi}\left(\frac{\Delta K}{2\sigma_y}\right)^2 \qquad (1)$$

where ΔK is the stress intensity factor amplitude and σ_y is the yield strength, equal 450 MPa for 7050-T7451 alloy.

The change of the cyclic plastic zone size, r_c, with the crack size using equation 1 is shown in Figure 9. In calculations two cases had to be considered. The first one is for small through thickness cracks, each of length L, emanating from the fasten hole of radius R. The stress intensity factor can be in this case approximated as [11,12]:

$$\Delta K = 3.36\,\Delta\sigma\sqrt{\pi L}\sqrt{\frac{2R+2L}{2R+L}} \qquad (2)$$

where $\Delta\sigma$ is stress amplitude which was equal 153 MPa. Another expression for ΔK have to be used for large cracks. In this case both cracks and the hole can be approximated as a through thickness center crack of length 2(R+L), Figure 3b, and ΔK is equal [13]:

$$\Delta K = \Delta\sigma\sqrt{\pi(R+L)}\left(\sec\frac{\pi(R+L)}{W}\right)^{1/2} \quad (3)$$

where W is double-hole specimen width. As Figure 9 shows, the size of the plastic zone at the crack initiation is about 10 μm. At the termination point, when the cracks are 2.5 to 3.5 mm long, it increases to about 250 μm. This is comparable to the typical grain size, which for the studied 7050-T7451 alloy is 138 μm for unrecrystallized grains. Thus, to see any possible damage due to fatigue, the TEM sample had to be perforated in a grain adjacent to the fatigue crack. Such accuracy is difficult to achieve, however we were able to perforate one of the samples within 10-20 μm from the plastic zone. The examination of that particular sample show no evidence of changes in the precipitate structure or debonding at the grain boundaries. Also the dislocation structure was no different than that of the bulk material. The dislocations were very difficult to locate but there was no tendencies to grouping and/or banding.

Above findings are consistent with other studies of dislocation structure in 7XXX alloys in low cycle fatigue. For instance, it was reported that even for the low strain amplitudes the grouping of dislocations can be seen as early as after few fatigue cycles[14]. Since the studied sample was exposed to 47,812 fatigue cycles, one would expect that some dislocation activities should occur. The fact that none has been observed can be attributed to the low maximum stress (only 38% of the yield strength) and to the partially recrystallized polygonized structure with stable subgrains. The material has thus few free dislocations to begin with thus the amount of "dislocation damage" resulted from fatigue would be much less than that for a unrecrystallized, cold-worked alloys. The effect of aging on the dislocation structure of 7050 alloy fatigued under low cycle, low strain amplitude conditions was investigated by Coyne and Starke[15]. They reported that going from underaged to peak aged to overaged conditions results in decreased

dislocation banding and in lowering of dislocation densities within the bands. Since the studied alloy was in the overaged conditions, this again explain lack of dislocation activities. All above results indicate that there is no fatigue damage in the precipitate and dislocation structures in the investigated 7050-T7451 alloy.

4. Summary

The microstructure in and adjacent to fatigue cracks of 7050 T7451 has been characterized to assess the amount of fatigue damage on the grain structure, second phase particles and dislocations levels. The following conclusions have been reached:

1. The fatigue cracks path is 60 to 95% transgranular with no preference towards unrecrystallized or recrystallized grains.
2. The intergranular portion of the crack path is preferentially between unrecrystallized and recrystallized grains.
3. Deflection of crack paths is controlled by the second phase particles. The number of particles on the crack path is significantly higher than the expected average.
4. No change in dislocation structure and no alterations of the precipitate structure was observed in the vicinity of the fatigue cracks.

5. Acknowledgments

The funding for this program was provided by the Office of Naval Research under contract N00014-91-J-1299. The authors are indebted to Dr. A. K. Vasudevan, the program manager, for valuable discussions and to Drs. P. E. Magnusen and R. J. Bucci from Alcoa Laboratories for providing all fatigued samples.

6. References

1. S. Suresh, *Fatigue of Materials*, Pub. Cambridge University Press 1991.
2. A. K. Vasudevan, R. D. Doherty and S. Suresh, Fracture and Fatigue Characteristics in Aluminum Alloys, pp 446 in *Aluminum Alloys - Contemporary Research and Applications, Treatise on Materials Science and Technology*, vol 31, ed. A. K. Vasudévan and R. D. Doherty, Pub. Acadamia Press, Inc., San Diego, 1989.
3. C. R. Owen, R. J. Bucci and R. J. Kegarise, Aluminum Quality Breakthrough for Aircracft Structural Reliablility, *Journal of Aircraft*, 26, (1989)178-184.
4. A. J. Hinkle, P. E. Magnusen, R. L. Rolf and R. J. Bucci, Effect of Microporosity on Notched Specimen Fatigue Life, pp 1467 - 1474 in *Proc. of 5th Int. Conference on Structure Safety and Reliability*, San Francisco, 1989.
5. J. R. Brockenbrough, R. J. Bucci, A. J. Hinkle, J. Liu, P. E. Magnusen and S. M. Miyasato, Role of Microstructure on Fatigue Durability of Aluminum Aircraft Alloys, F33615-92-C-5915, Alcoa Center, PA 1993.
6. M. A. Przystupa, J. Zhang and A. J. Luévano, Development of the Microstructure Based Stochastic Life Prediction Models, N00014-91-J-1299, University of California, Los Angeles, 1992.
7. B. B. Mandelbrot: *Fractal Geometry of Nature*, Pub. W. H. Freeman and Company, New York, NY, 1982.
8. E. L. Crow, F. A. Davis and M. W. Maxfield, pg 37 in *Statistical Manual*, Pub. Dover Publications, Inc., New York, 1960.
9. M. A. Przystupa, J. Zhang and A. J. Luévano, Development of the Microstructure Based Stochastic Life Prediction Models, N00014-91-J-1299, University of California, Los Angeles, 1991.

10. J. Zhang, A. J. Luévano and M. A. Przystupa, Quantitative Analysis of Heterogeneous Grain Structure on Plane Sections, *Scripta Metallurgica et Materialia*, 26,(1992) 1061 - 1066.

11. R.C. Shah, Stress Intensity Factors for Through and Part-Through Cracks Originating at Fastener Holes, pp. 429-459 in *Mechanics of Crack Growth*, ASTM STP 590, American Society for Testing and Materials, 1976,.

12. O. L. Bowie, *Journal of Mathematics and Physics*, 35, (1956) 60-71.

13. D. Broek, pg 85 in *Elementary Engineering Fracture Mechanics*, 4th edition, Pub. Kluwer Academic Publishers, Dordrecht, The Netherlands, 1991.

14. C. Laird, Mechanisms and Theories of Fatigue, pp 149 - 204 in *Fatigue and Microstructure*, Pub. American Society for Metals, Metals Park, Ohio, 1978.

15. E. J. Coyne, Jr. and E. A. Starke, Jr., The effect of microstructure on the fatigue crack growth behaviour of an Al-Zn-Mg-(Zr) alloy, *International Journal of Fracture*, 15[5],(1979) 405 - 417.

7. Tables

Table 1. Crack lengths and roughness parameters.

Crack Identification	Section	Projected Length (μm)	Actual Length (μm)	Profile Roughness Parameter
#1	Surface	1937	2400	1.24
	1/3 thickness	2771	3277	1.18
	2/3 thickness	2773	3307	1.19
#2	Surface	3292	3635	1.10
	1/3 thickness	3600	4037	1.12
	2/3 thickness	3433	4171	1.22

Table 2. Percentage of crack length in various regions of grain structure.

Sample		Transgranular Crack Path			Intergranular Crack Path				
Crack No.	Section	Unrecr. (%)	Recrys. (%)	Total (%)	u/r bou. (%)	r/r bou. (%)	u/u bou. (%)	Subgr. (%)	Total (%)
#1	front surface	76.1	12.3	88.4	2.2	1.5	-	7.9	11.6
	1/3 thickness	5.4	5.9	60.2	25.8	7.2	5.1	1.7	39.8
	2/3 thickness	63.4	22.4	85.8	12.6	-	1.5	-	14.2
	back surface	65.6	12.8	78.4	12.8	8.8	-	-	21.6
#2	surface	65.8	26.2	92.0	8.0	-	-	-	8.0
	1/3 thickness	75.7	18.5	94.2	5.8	-	-	-	5.8

u/u = unrecrystallized/recrystallized
r/r = recrystallized/recrystallized
u/u = unrecrystallized/unrecrystallized

Table 3. Number of intercepts of scan lines and crack path with second phase particles.

Crack Number	Section	Straight Line (No./μm)	Crack Path (No./μm)	Significance Level (%)
#1	surface	$9.9 \times 10^{-4} \pm 6.5 \times 10^{-4}$	2.0×10^{-3}	< 0.1
	1/3 thickness	$8.7 \times 10^{-4} \pm 4.5 \times 10^{-4}$	2.1×10^{-3}	< 0.1
	2/3 thickness	$9.4 \times 10^{-4} \pm 5.8 \times 10^{-4}$	1.6×10^{-3}	< 0.1
#2	surface	$8.0 \times 10^{-4} \pm 5.8 \times 10^{-4}$	1.3×10^{-3}	< 0.1
	1/3 thickness	$1.2 \times 10^{-4} \pm 5.8 \times 10^{-4}$	1.9×10^{-3}	< 0.1
	2/3 thickness	$1.0 \times 10^{-3} \pm 4.1 \times 10^{-4}$	2.2×10^{-3}	< 0.1

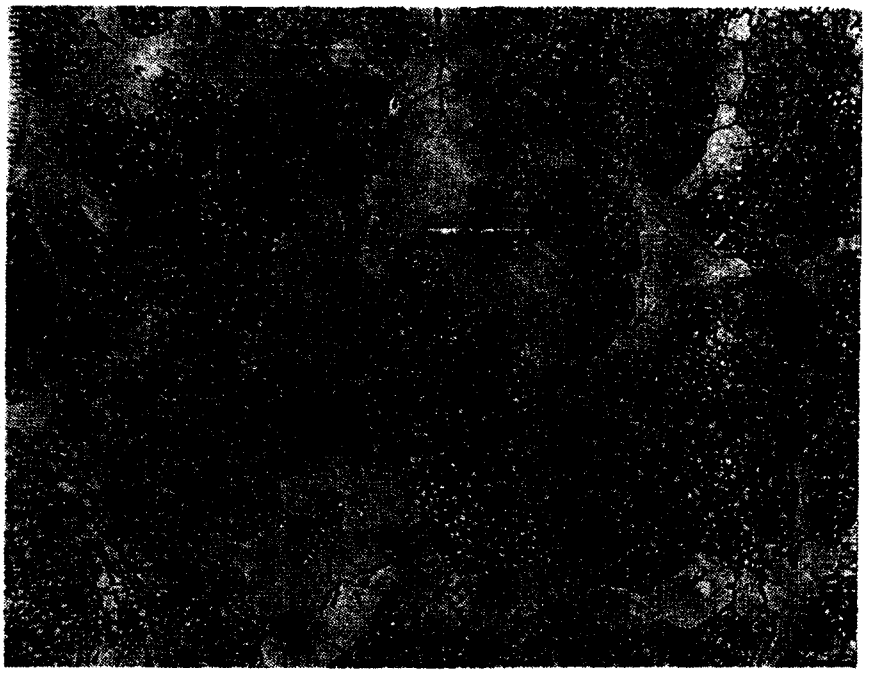

Figure 1. Micrograph showing recrystallized and unrecrystallized grains in 7050-T7451 aluminum alloy.

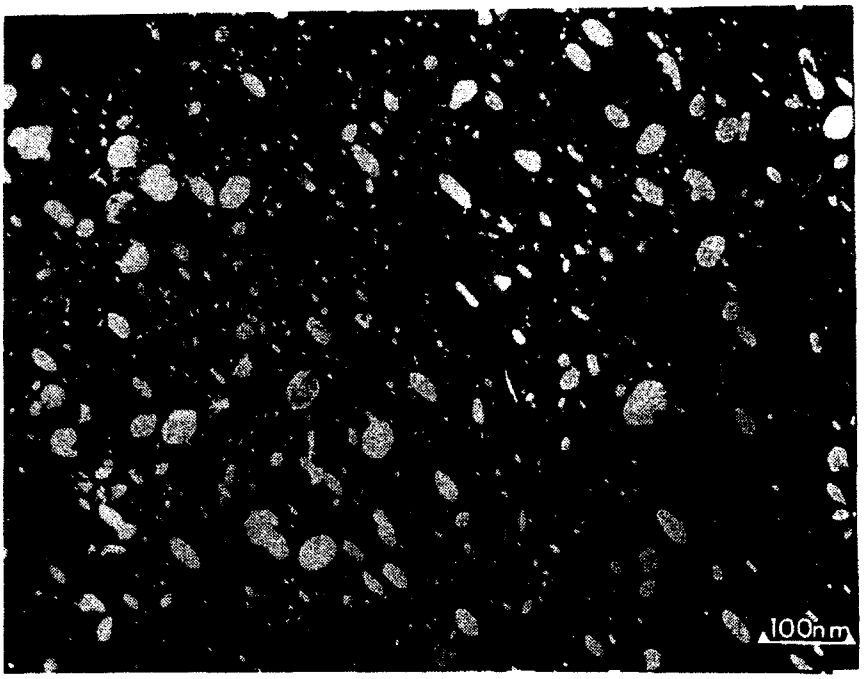

a)

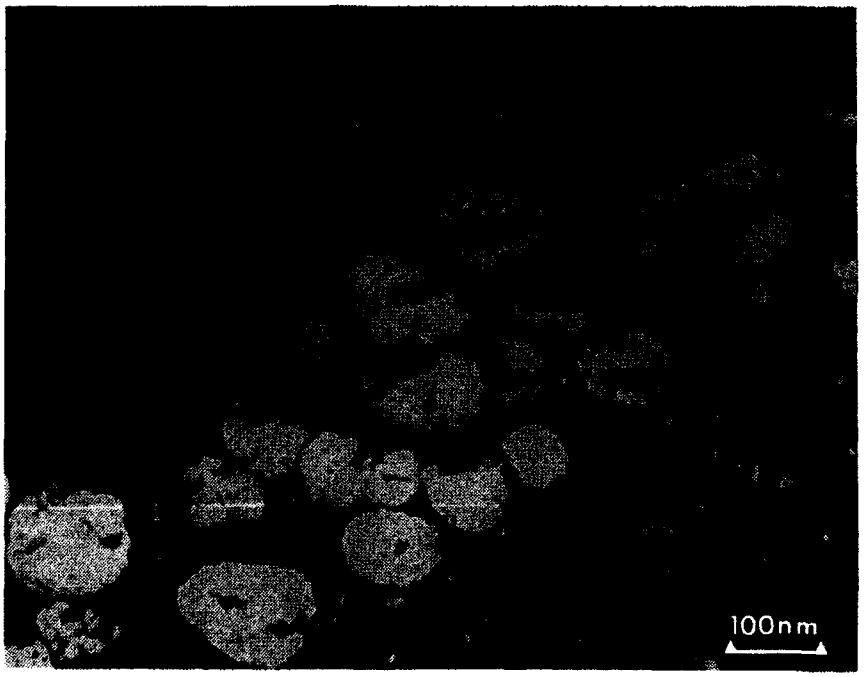

b)

Figure 2. Precipitate microstructure of 7050-T7451 a) grain boundary precipitates and b) matrix precipitates.

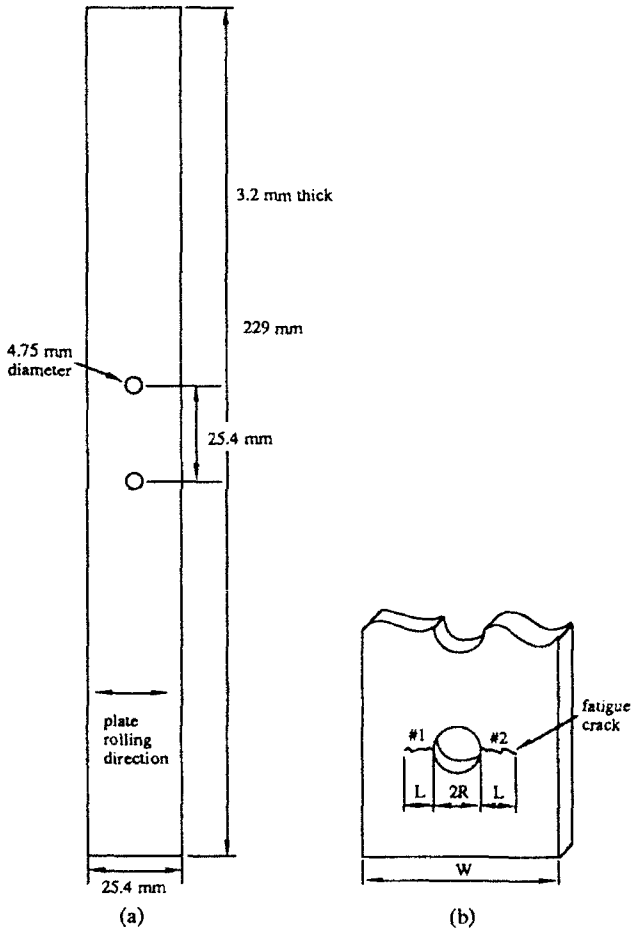

Figure 3. Fatigue samples a) two-hole fatigue sample and b) schematic of secondary fatigue cracks

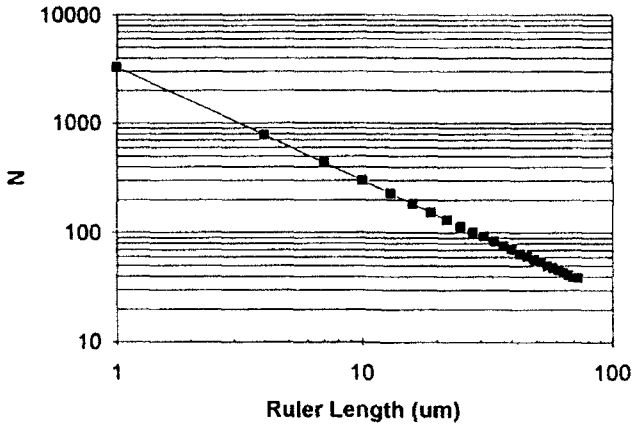

Figure 4. Plot for determining fractal dimensions of fatigue crack #2, surface region.

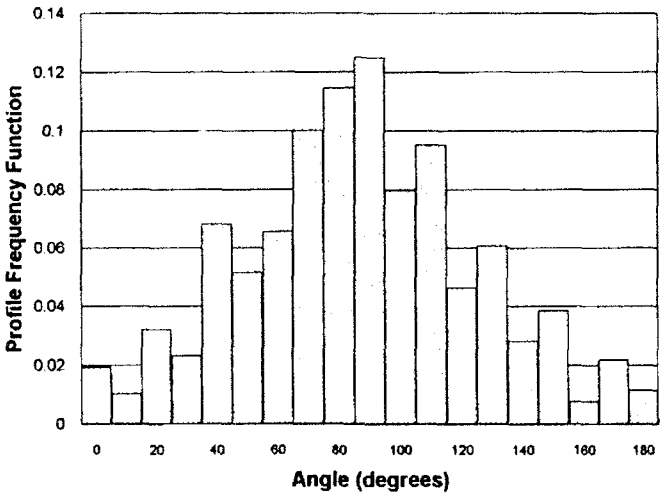

Figure 5. Distribution of angular orientation of crack segment, crack #2, surface section.

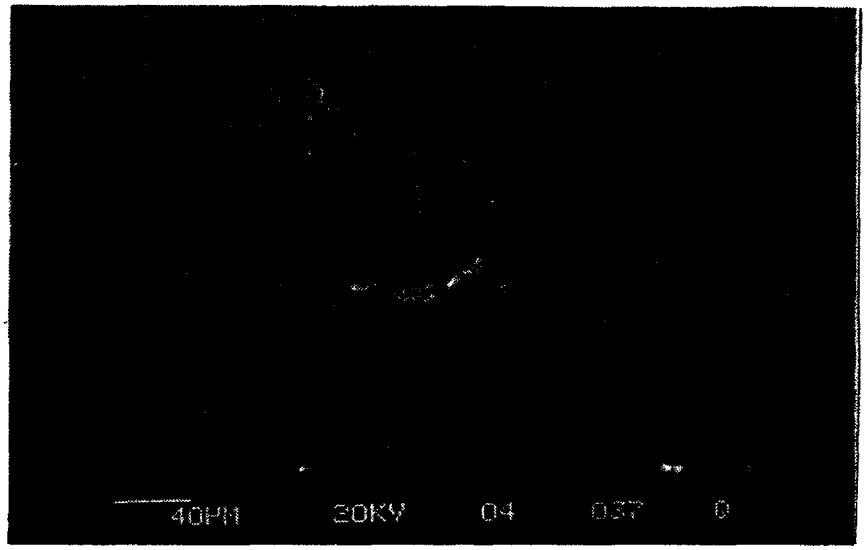

a)

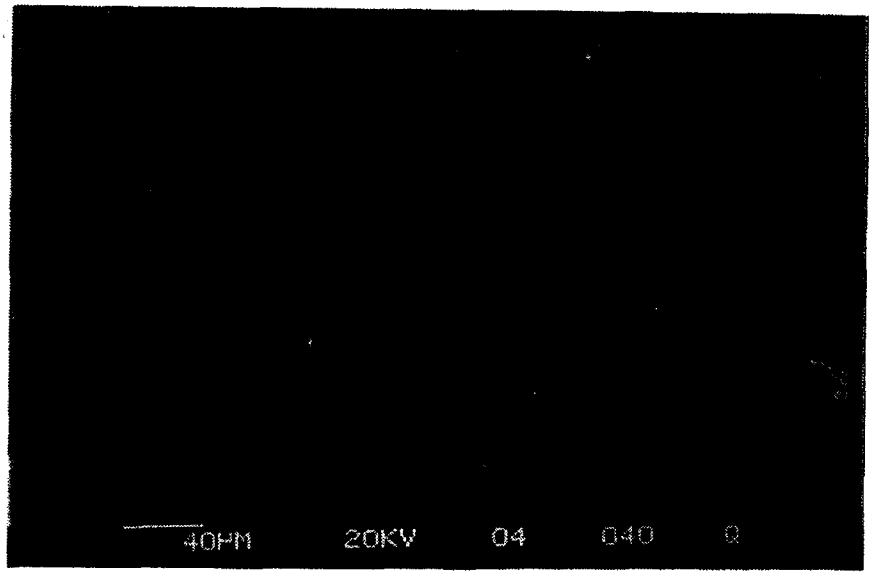

b)

Figure 6. Examples of branching of fatigue cracks in 7050-T7451 alloy a) branches propagating through constituent particles b) branches propagating along grain boundaries.

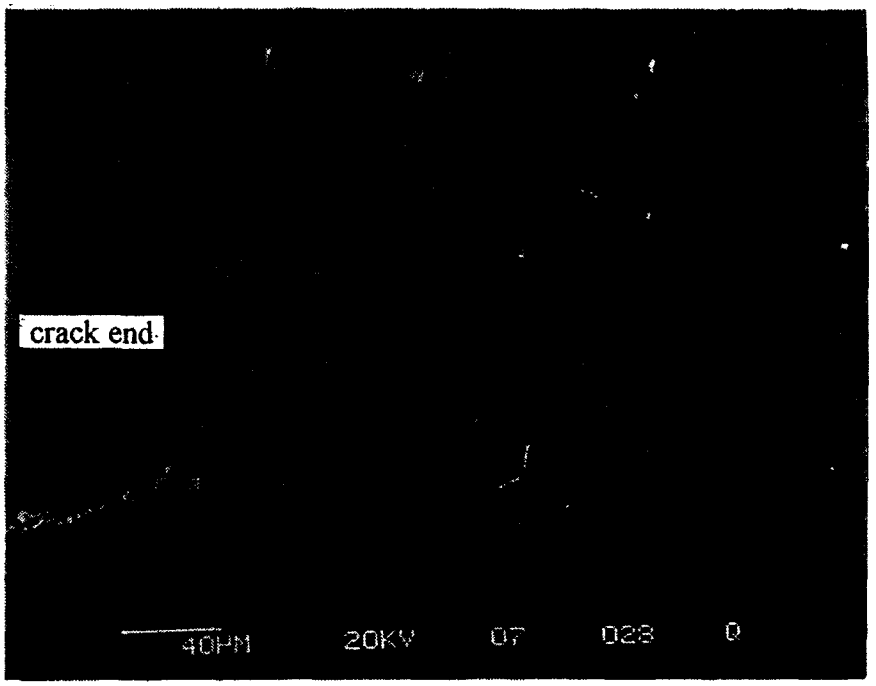

a)

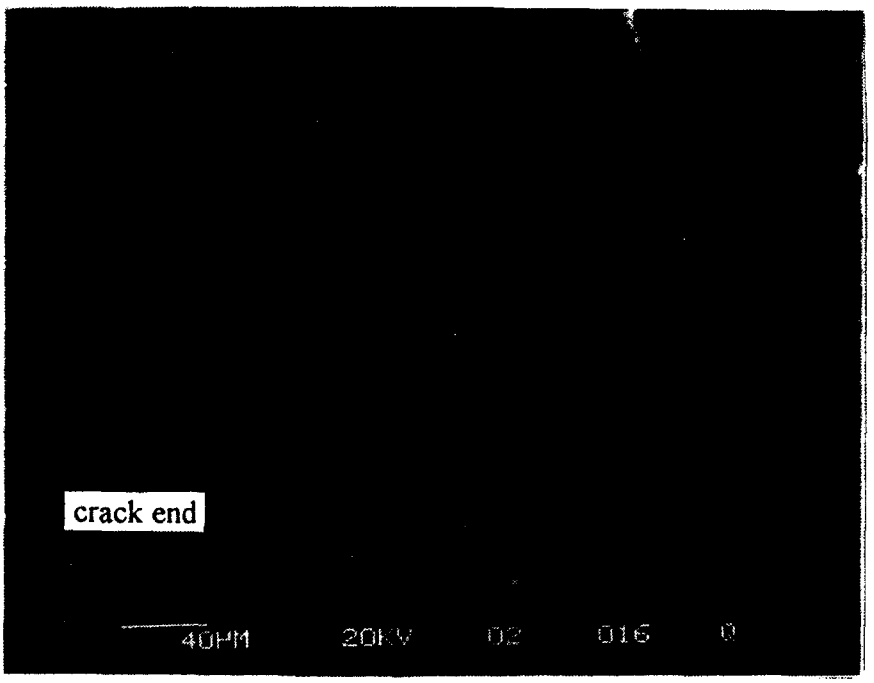

b)

Figure 7 Examples of microcracks in the vicinity of main crack
Arrows indicate end of fatigue crack

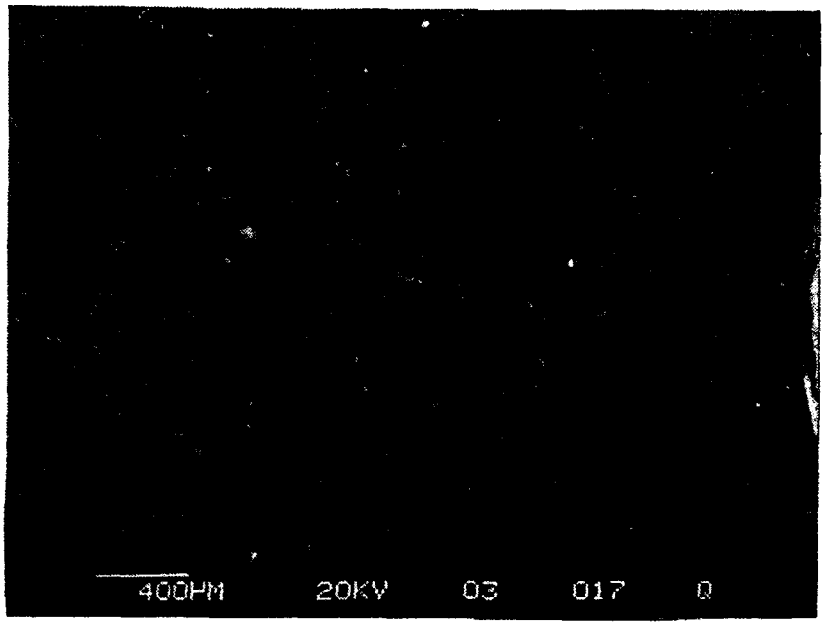

Figure 8. Example of micrograph used to calculate number of particles intercepted by scan lines and crack in 7050-T7451 aluminum alloy.

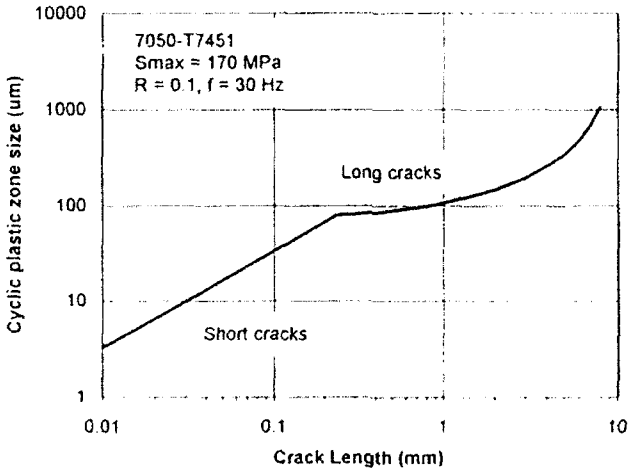

Figure 9. Changes in plastic zone size with crack length in 7050-T7451 aluminum alloy.